Science Bulletin 66 (2021) 2225–2237

Contents lists available at ScienceDirect

Science Bulletin

journal homepage: www.elsevier.com/locate/scib

Science Bulletin
www.scibull.com

Article

Schizophrenia risk-gene *Crmp2* deficiency causes precocious critical period plasticity and deteriorated binocular vision

Yuan Zhang [a], Li Yao [a], Xiang Li [a], Meizhen Meng [a], Ziwei Shang [a], Qin Wang [b], Jiaying Xiao [b], Xiang Gu [a], Zhiheng Xu [b], Xiaohui Zhang [a,*]

[a] State Key Laboratory of Cognitive Neuroscience & Learning, IDG/McGovern Institute for Brain Research, Beijing Normal University, Beijing 100875, China
[b] State Key Laboratory of Molecular Developmental Biology, Institute of Genetics and Developmental Biology, Chinese Academy of Sciences, Beijing 100101, China

ARTICLE INFO

Article history:
Received 14 August 2020
Received in revised form 15 December 2020
Accepted 29 January 2021
Available online 6 February 2021

Keywords:
Critical period plasticity
Collapsin response mediator protein-2 (*CRMP2*)
Excitation-inhibition balance
Primary visual cortex
Binocular depth perception
Schizophrenia

ABSTRACT

Brain-specific loss of a microtubule-binding protein collapsin response mediator protein-2 (*CRMP2*) in the mouse recapitulates many schizophrenia-like behaviors of human patients, possibly resulting from associated developmental deficits in neuronal differentiation, path-finding, and synapse formation. However, it is still unclear how the *Crmp2* loss affects neuronal circuit function and plasticity. By conducting *in vivo* and *ex vivo* electrophysiological recording in the mouse primary visual cortex (V1), we reveal that CRMP2 exerts a key regulation on the timing of postnatal critical period (CP) for experience-dependent circuit plasticity of sensory cortex. In the developing V1, the *Crmp2* deficiency induces not only a delayed maturation of visual tuning functions but also a precocious CP for visual input-induced ocular dominance plasticity and its induction activity – coincident binocular inputs right after eye-opening. Mechanistically, the *Crmp2* deficiency accelerates the maturation process of cortical inhibitory transmission and subsequently promotes an early emergence of balanced excitatory-inhibitory cortical circuits during the postnatal development. Moreover, the precocious CP plasticity results in deteriorated binocular depth perception in adulthood. Thus, these findings suggest that the *Crmp2* deficiency dysregulates the timing of CP for experience-dependent refinement of circuit connections and further leads to impaired sensory perception in later life.

1. Introduction

Human schizophrenia (SCZ) is a complex mental disorder with a high degree of heritability and environmental susceptibility. This psychiatric disease is generally thought to be associated with many dysregulated neurodevelopmental processes involving aberrant synaptic connections and function in very early life [1]. Human genetic studies have suggested that a gene encoding the collapsing response mediator protein 2 (CRMP2, or DPSYL2 in human), located at chromosome region 8p21, is associated with schizophrenia [2] and reduced expression of *Dpsyl-2* was found in the postmortem brain of schizophrenia patients [3,4]. The protein CRMP2 is an important component of neural cell cytoskeletons and is highly expressed in neuronal soma, axons, and dendrites [5]. Many experimental studies have suggested its roles in regulating microtubule dynamics associated with neuronal cell migration and path-finding, as well as neural network plasticity [6].

CRMP2 is preferentially expressed in highly plastic brain regions, such as the neocortex, hippocampus and cerebellum in the mouse brain, differing from expression patterns of four other CRMP family members (CRMP1, CRMP3, CRMP4, and CRMP5) [5]. Accumulating evidence has suggested its important roles in regulating the formation, maturation and plasticity of synaptic circuits [6]. For an example, we recently found that brain-specific *Crmp2*-knockout (*Crmp2*-KO or *Crmp2*$^{-/-}$) mice exhibited apparent deficits in neuronal dendritic arborization, synapse formation, aberrant glutamatergic receptor composition, and activity-dependent long-term potentiation of synaptic transmission in the hippocampus [7]. More importantly, these *Crmp2*-KO mice recaptured most schizophrenia-like symptoms, including the augmented psychomotor agitation, social withdrawal, pre-pulse inhibition deficit and impaired hippocampus-dependent learning and memory [7].

It is generally accepted that formation and maturation of many brain functions crucially rely on experience-dependent rearrangements of their synaptic connections during defined postnatal critical periods (CPs), known as the CP plasticity [8,9]. Interestingly, the level of *Crmp2* expression in the brain was substantially high

* Corresponding author.
E-mail address: xhzhang@bnu.edu.cn (X. Zhang).

https://doi.org/10.1016/j.scib.2021.02.011
2095-9273/

during similar postnatal periods (e.g., postnatal days (P) 10–30 [10,11]) and CRMP2 was found to actively regulate neuronal structural changes [12]. Thus, it is of interest to examine whether CRMP2 is involved in functional maturation and plasticity of a neural circuit during the CP *in vivo* and how the *Crmp2* loss could lead to impaired developmental plasticity and brain function.

In the present study, by examining a classic form of CP plasticity – visual input-induced ocular dominance (OD) plasticity of the primary visual cortex (V1) – in the *Crmp2*$^{-/-}$ mice after eye-opening, we showed that brain-specific loss of *Crmp2* can induce an aberrant CP, with the precocious onset timing and shortened duration, for experience-dependent cortical plasticity. An accelerated maturation of cortical inhibitory transmission and the resulting excitation/inhibition (E/I) balance in cortical circuits shortly after eye-opening, following the *Crmp2* loss, accounts for the precocious CP plasticity. This dysregulation of CP plasticity of developing V1 further could lead to a degraded function of depth perception in adulthood. Thus, our findings not only reveal a novel role of CRMP2 in the regulation of early experience-dependent sensory circuit plasticity and functional maturation, but also suggest that dysregulation of the CP plasticity is responsible for persistent sensory function deficits found in neurodevelopmental diseases such as schizophrenia.

2. Materials and methods

2.1. Animal preparation

All surgical and experimental procedures were performed with the protocols approved by the Animal Care and Use Committee of the State Key Laboratory of Cognitive Neuroscience and Learning, Beijing Normal University (IACUC-BNU-NKLCNL-2016-02) and the Institute of Genetics and Developmental Biology, Chinese Academy of Sciences. Wild-type C57BL/6 and transgenic mice were raised in the Animal House with 12/12-h light/dark cycles. Mice at P14–70 were used for the experiments. Both male and female mice were used.

Monocular deprivation (MD) of visual input was achieved by suturing the eyelid of one eye. The eyelid suture was made under isoflurane anesthesia (1%–3% in oxygen), as described previously [13]. After recovery from anesthesia, the animals were exposed to regular 12/12-h light/dark rhythms. The eyelid suture was checked daily to ensure that the sutured eye remained closed and uninfected. Animals showing an eye infection or an eyelid suture loose during the MD period were not used in the experiments.

Brain surgery and *in vivo* electrophysiological recordings were performed in mice that were anesthetized by an intraperitoneal injection of ketamine (50 μg/g body weight)/medetomidine (0.6 μg/g) and mounted on a custom-built mouse stereotaxic device in most experiments. The animal heart rate and body temperature were monitored to check anesthesia states and if necessary, an additional 2/3 to 1/2 of the initial dose of anesthesia was given to sustain stable anesthesia. Body temperature was maintained at 37 °C by a homeostatically controlled heating pad (RWD Life Science, Shenzhen, China). For the recording, a craniotomy was made over the binocular zone (approximately 2.8 mm lateral lambda) of the mouse V1 [8,13], and the dura mater was carefully removed. Warm saline and eye drops were frequently applied onto the exposed cortical surface and the eyes respectively when necessary.

For behavior tests, mice at adult ages (postnatal 7.5–8 weeks) were housed in standard cages (28 cm × 18.5 cm × 15 cm). For some mice, their whiskers were trimmed in order to examine possible influence of tactile inputs on animal performance in the depth exploration task. The behavioral tests were conducted within 1 or 2 days after the whisker trimming.

2.2. Visual stimulation

Visual stimuli were generated by a custom-developed software program by the LabView system and the MATLAB, and displayed on a 20-inch cathode ray tube (CRT) monitor (Sony Multiscan G520, Sony Corporation, Tokyo, Japan; 40.5 cm × 30.5 cm; refresh rate, 60 Hz; maximum luminance, 80 Candela (cd)/m^2). The CRT monitor was placed 20 (±1) cm in front of the mouse, covering approximately 105° × 80° of the mouse front visual field. To stimulating one eye only, a custom-made conical black eye-shield was used to cover an eye alternatively in the experiment.

Full-field drifting sinusoidal gratings (at 100% contrast level; spatial frequency, 0.02 Hz/degree; temporal frequency, 2 Hz; 8 directions) were presented for 4 s in a pseudorandom sequence with 4 trial repeats at each orientation to assess orientation tunings of recorded V1 neurons. Seven different spatial frequencies ranging from 0 to 0.64 cycle per degree (cpd, with 2 Hz temporal frequency) were set to measure the spatial frequency selectivity. In the experiments of measuring the binocular input synchrony of V1 binocular zone (V1B) neurons, full-field static gratings with defined optimal orientation at 3 different spatial phases (0°, 120°, and 240°; spatial frequency, 0.013 Hz/degree) were presented for 0.3 s in a pseudorandom sequence with 40 trial repeats at each phase [13]. The intervals for presenting static gratings varied in the range of 0.9–1.3 s. Same full-field static gratings were used in the experiments for separating excitatory and inhibitory conductance in visual responses *in vivo* (0°, 120°, 180°, 240°, and 300° with 20 repeats at each phase). The 8 × 8 grids of a flashing square (9–11° pixel size; 50-ms duration spaced by 200-ms blank) were presented a sparse noise model to map the receptive field of recorded V1B neurons, and stimulation at each position had 50–100 repetitions.

2.3. In vivo extracellular and whole-cell recording

Extracellular single-unit recording and whole-cell recording followed the methods described in previous studies of mine [13] and other groups [14,15]. Briefly, extracellular recordings were made using the borosilicate glass micropipettes in the V1B (~2.8 mm lateral from the lambda; [8]) in a brain hemisphere that was contralateral to the deprived eye, with 4–8 penetrations spanning across the mediolateral extension of the V1B. Micropipettes were filled with the normal saline, and its resistances were 6–8 MΩ.

For the current-clamp whole-cell recording, micropipettes were filled with an internal solution containing (in mmol/L): 140 K-concatenate, 2 $MgCl_2$, 10 N-2-hydroxyethylpiperazine-N-2-ethane sulfonic acid (HEPES), 0.05 $CaCl_2$, 0.4 ethylene glycol-bis (2-aminoethylether)-N,N,N′,N′-tetraacetic acid (EGTA), 4 adenosine 5′-triphosphate magnesium salt (Mg-ATP), 0.4 guanosine 5′-triphosphate sodium salt hydrate (Na_2GTP), and 10 Na_2-phosphocreatine, pH 7.20 (adjusted with KOH, ~0.29 osmoles per liter, OSM). For the voltage-clamp whole-cell recording, the internal solution contained (in mmol/L) 120 Cs-methanesulfonate, 20 KCl, 10 EGTA, 2 $MgCl_2$, 2 Na_2ATP, 10 HEPES, and 5 QX-314 (~0.29 OSM). During voltage-clamp recording, membrane potentials of recorded neurons were set at least three different values ranging from −70 to 15 mV for isolating excitatory and inhibitory conductance. Micropipettes were tip-filled with internal solution and then back-filled with the internal solution containing 300 μg/mL amphotericin B [16], and had a resistance in the range of 3–6 MΩ.

All electric signals were recorded with an Axon MultiClamp 700B amplifier (Molecular Devices, San Jose, USA), filtered at 5 or

10 kHz (low pass), digitized by a Digidata 1440A converter board (Molecular Devices), and acquired by computer for further analysis. In the voltage-clamp recording, the junction potential of 10-mV was corrected. All recorded neurons resided in a depth range of 200–500 μm below the pia based on the manipulator microdriver reading (Sutter Instrument, Novato, USA), and thus most recorded neurons were within the cortical layers II/III and IV. The whole-cell recording experiment included total 97 neurons, among which 76 and 21 cells were recorded with and without the sodium channel blocker QX-314, respectively.

2.4. Visual cortical slice electrophysiology ex vivo

The procedures of preparing visual cortical slices from *Crmp2*$^{+/+}$ or *Crmp2*$^{-/-}$ mice, aged P15–17 or 27–29, and whole-cell recording on excitatory pyramidal cells (PCs) within the layer II/III followed the methods described in our previous study [17]. Detailed descriptions of cortical slice preparation and recording were shown in the Supplementary materials (online).

2.5. Immunohistochemistry and confocal imaging

The procedure for the preparation of visual cortical sections from P14–20 or P25–31 mice and subsequent immunostaining followed a method described in our previous studies [18], and its details were shown in the Supplementary materials (online).

2.6. Behavioral tests for depth perception

The size of the visual-cliff box was 52 cm × 30.5 cm × 52 cm (length × width × height), and a vertical wall (36 cm high and 1 cm wide) was in the middle position to divide the box into two chambers. Two acrylic glass plates with a pattern of 1.5-cm red/white squares or checkered boxes were placed in both chambers, and their heights were independently set to produce the depth difference. The plates were illuminated from the bottom with LED lamps to achieve the same luminance without apparent visual disturbance between the two chambers. A tele-camera was placed in a center position ~50 cm above the apparatus to have a full view of the animal behaviors (in 30 frames/s). The videos were acquired and clipped by the software VirtualDub (http://virtualdub.org/). All tests were conducted in a double-blind manner and carried out in a separated, quiet environment. The visual-cliff box was covered with hoods. Surfaces of the plates, platforms, and four sidewalls were cleaned with halimide solution (1:300) between trials.

2.6.1. Depth exploration test

A transparent acrylic board (size: 52 cm × 30.5 cm) spanned the two chambers as a base platform, and separated checkered-box plates in the two chambers were placed 0 and 15 cm underneath the base platform as the shallow and deep sides, respectively. The shallow and deep sides related to the mouse itself were switched randomly from trial to trial. Each animal was placed on the shallow side, and the spontaneous exploring activities of the mice on each side of the arena were recorded. The trial ended after 3 min and was analyzed offline using the MATLAB-based open-source program Optimouse [19]. Each animal was tested only once.

2.6.2. Depth descent test

Mice were trained to conduct a two-alternative forced-choice task. To avoid confounding effects derived from tactile stimulation, the patterned floor was positioned 6 cm below the board basement as a shallow side, and Plexiglas plates were removed. Mice were first conditioned to distinguish a high differential depth with great reliability before the limit of this ability could be assessed. The depth descent test consisted of three phases: the preadaptation phase, training phase, and final testing phase. In the preadaptation phase, mice were habituated to the box, without any depth difference between the two plates in the two chambers, for five 10 min-trials twice a day with 5-h intervals in between. In the training phase, water-deprived mice were trained to descend from a narrow center wall (1 cm width) to the shallow side plate within 2 min under a condition with the maximal depth difference (15 cm) between the two plates in all trials. A small amount of yogurt (< 0.5 mL per time) was given to animals only when the animal made the correct choice, and for the situation of no action (regarded as "no choice") or the accidental fall-off of animals, mice were immediately put back into the cage to wait for subsequent trials. Only those mice exhibiting an > 80% correct rate after 20–30 training trials were subjected to the next phase. In the final testing phase, the trained animals were tested for five trials per depth difference, 15, 10, 5, 3, and 1 cm, in a pseudorandom order. Each trial was restricted to 2 min, and the "no-go" trials were counted. No rewards were received by mice in this testing phase. Note that no animal fell off the standing point in any tested trials. The shallow and deep sides were randomly switched between the two chambers among trials.

2.7. Data analysis

All experiments, including the recording, immunostaining, and behavioral tests, were carried out in a double-blind manner in which the experimenters did not know the genotypes or the treatments of the mice prior to and during the tests. The data were then pooled accordingly based on individual genotypes or treatments after the tests.

2.7.1. Visual function analysis

The orientation selectivity index was computed using the following equation [20]:

$$global\,OSI = \left(\sqrt{\sum (R(\theta_i) \times \sin(2\theta_i))^2 + \sum (R(\theta_i) \times \cos(2\theta_i))^2}\right) / \sum (R(\theta_i)), \quad (1)$$

and the direction selectivity index was computed using the following equation:

$$global\,DSI = \left(\sqrt{\sum (R(\theta_i) \times \sin(\theta_i))^2 + \sum (R(\theta_i) \times \sin(\theta_i))^2}\right) / \sum (R(\theta_i)), \quad (2)$$

where θ_i, is the angle of the moving direction of the grating and $R(\theta_i)$ is the spike response amplitude (with baseline subtracted) at angle θ_i [21]. The receptive field estimation was performed by reversely correlating the averaged spike rate with the flashing squares in the 8 × 8 grid, and RF spatial and temporal properties were analyzed [22]. The spatial RF was calculated by fitting the frame with the largest variance with the following 2D Gaussian functions:

$$RF(x,y) = Ae^{-\left[\frac{x'^2}{2(\sigma_x^2)} + \frac{y'^2}{2(\sigma_y^2)}\right]}, \quad (3)$$

$$x' = (x - x_0) \times \cos\theta + (y - y_0) \times \sin\theta, \quad (4)$$

$$y' = (x - x_0) \times \cos\theta + (y - y_0) \times \sin\theta, \quad (5)$$

where $RF(x, y)$ represents the spike rate response when the flashing square was presented at site (x, y), A is the spike rate of the RF response, x and y determine the two axes of RF, θ is the orientation of RF, and (x_0, y_0) represents the center of RF. The spatial territory of RF is estimated based on two times the standard deviation (SD) of the fitted 2D Gaussian function. For the analysis of the ocular preference in the recording, the contralateral bias index (CBI) was classified as 1 when the preference was driven exclusively by the

ipsilateral eye and as −1 when the preference was driven exclusively by the contralateral eye. The classic 7-point scale was used to convert *CBI* values into OD scores. The *CBI* was quantified as follows:

$$CBI = [(n_1 - n_7) + (2/3) \times (n_2 - n_6) + (1/3) \times (n_3 - n_5)]/2N, \quad (6)$$

where N is the total number of cells and n_x is the number of cells with an OD score equal to s on a 7-point scale [8]. For each recorded visual cell in the V1B, the degree of OD was quantified by an index (*ODI*):

$$ODI = (C - I)/(C + I), \quad (7)$$

where C and I represent rates of spiking activity evoked by visual stimuli presented to the contra- and ipsilateral eyes, respectively, after a baseline subtraction.

2.7.2. Analysis of in vivo whole-cell recording data

For the analysis of subthreshold PSP responses, we adapted the same method used in our previous work [13]. For separation of excitatory and inhibitory input conductance (*Ge* and *Gi*) *in vivo*, we mainly adopted the methods used in the previous studies by Wehr and Zador [23] and ours [24]. Static gratings-evoked postsynaptic currents, recorded at 3 or 4 different clamped membrane potentials, were further averaged by repeats (twenty repeats for each spatial phase of static grating) and smoothed by high-pass filtering [25]. The detailed calculation of *Ge* and *Gi* was shown the Supplementary materials (online).

The E/I ratio was calculated based on the peak magnitudes or the areas of evoked *Ge* and *Gi*, respectively. We adopted a previous method used by Monier et al. [26] to compare magnitudes of *Ge* and *Gi* of a neuron for each stimulation trial, in which six static gratings were given to the contra- or ipsi-lateral eye. For the mean E/I ratio for individual recorded neurons, calculated E/I ratios for each trial were averaged according to the stimuli to contra- and ipsi-lateral eye, respectively, and thus each neuron yielded two values of the mean E/I ratio. Data for each genotype group were from 4 to 6 mice.

2.7.3. Behavioral result analysis

For the depth exploration behavior test, the enrichment score ($E_{\text{-score}}$) was calculated using the following equation [19]:

$$E_{-\text{score}} = (\textit{Actual exploration time in the zone})/(\textit{Excepted time in the zone}), \quad (8)$$

The excepted time is defined as:

$$\textit{Excepted time} = T_t \times \textit{Area}_{\text{zone}}/\textit{Area}_{\text{arena}}, \quad (9)$$

where T_t is the total time of the recording for analysis, $Area_{\text{zone}}$ is the area of selected zone and $Area_{\text{arena}}$ is the area of the box (area sum of three zones). The *E-score* bias index (*EBI*) was calculated as follows:

$$EBI = (E_{\text{shallow}} - E_{\text{deep}})/(E_{\text{shallow}} + E_{\text{deep}}), \quad (10)$$

where E_{shallow} and E_{deep} are the enrichment score for the shallow and deep zones that the mouse explored. The surfaces of both zones, the starting board, and the walls were cleaned after every single trial. The detailed posture analysis is based on frame by frame labeling of body center to nose (body length), and then checked and corrected manually afterwards using the same open-source program Optimouse [19]. For the depth descent test, the preference for shallow or deep side was defined as lingering on one side with full body on the checkered-box labeled plate in five trials. The choice index (*CI*) for each mouse was calculated as follows:

$$CI = (n_{\text{shallow}} - n_{\text{deep}} - n_{\text{ng}})/N_{\text{trials}}, \quad (11)$$

where n_{shallow}, n_{deep}, and n_{ng} are the numbers of mice staying on the shallow side, the opposite side, "no-go" behaviors, respectively, and N_{trials} is the total trial number per depth.

Data are presented as mean ± SD unless otherwise stated in text and figure legends. The detailed information of statistical tests for significant difference between two data sets is listed in the figure legends, along with the number of examined cells or animals.

3. Results

3.1. CRMP2 deficiency delays maturation of orientation/direction tunings of V1 neurons

Brain-specific *Crmp2* deletion was achieved by crossing the $Crmp2^{flox/flox}$ mice with the *Nestin-Cre* mice, as described in our previous study [7]. Although these $Crmp2^{-/-}$ mice had normal cortical thickness, lamina, and neuron density [7], it was not clear whether cortical functions in CRMP2-deficient circuits are developed normally or not. Thus, in this study, we firstly conducted *in vivo* extracellular single-unit recordings on V1B to assay their basic visual functions in the $Crmp2^{+/+}$ (control) and $Crmp2^{-/-}$ littermates, respectively, at P14–21 (juvenile), P24–32 (adolescence), or P65–70 (adult). The drifting gratings at eight directions or the 8 × 8 grids of flashing squares were used to measure various tuning functions (Fig. 1a–d). We found that, within 1 week after eye-opening (P14–21), V1B neurons in the *Crmp2*-KO mice exhibited much weaker orientation/direction tunings than that in the control littermates, as indicated by plots of the cumulative distribution of the global orientation or direction selectivity index (*gOSI* and *gDSI*) of all recorded neurons in the two genotype groups (Fig. 1e). However, the latter difference in *gOSI* or *gDSI* strengths was not evident when animals reached the stage of P24–32 (Fig. 1f) or the adult stage (Fig. S1a online).

In contrast, the spatial size of receptive fields (RFs) of recorded V1B neurons were largely same between the two genotype groups at all three ages (Fig. 1a–d, g, and Fig. S1b online for adult animals). Moreover, spiking responses of all tested V1B neurons consistently showed a similar preference to low spatial-frequency stimuli in both genotypes (Fig. 1h and Fig. S1c online).

These neurophysiological results directly indicate that the *Crmp2* deletion could cause a delayed maturation of orientation/direction tunings in developing V1B neurons within the first week after eye-opening, but the *Crmp2*-deficient V1B neurons still develop similar tuning strengths as the normal V1 neurons in the later postnatal stages.

3.2. Crmp2 loss causes a precocious CP for ocular dominance plasticity in developing mouse V1

We next examined whether the *Crmp2* loss affects early experience-dependent circuit plasticity by assaying the classic monocular deprivation (MD)-induced OD shifts (or plasticity) of developing V1B neurons during the well-defined postnatal CP (P21–35) in mice [27].

To determine the timings of CP onset and closure, we performed the 4-day MD of one eye input by eyelid suturing at various days beginning at a day within the period of P15–20 (the first week after eye-opening), P21–30 (in the normal CP), or > P65 (adult). Respective OD shifts following the MD at the three different periods were indicated by the 7-scale histograms or the cumulative distribution of *ODI* measured from V1B neurons in the contralateral V1. The results indicate that the control $Crmp2^{+/+}$ mice had a same normal CP timing as that of the wild-type (WT) mice, in which the OD shift was clearly observed when the MD was made at P26, but not for MD at P15 (Fig. 2a, b) or adulthood (Fig. S1d online). On the contrary, the $Crmp2^{-/-}$ littermates exhibited OD shifts only when the MD was conducted around P15, but not for MD at the later stages, such as at P26 (Fig. 2c, d) and adulthood (Fig. S1e online). These

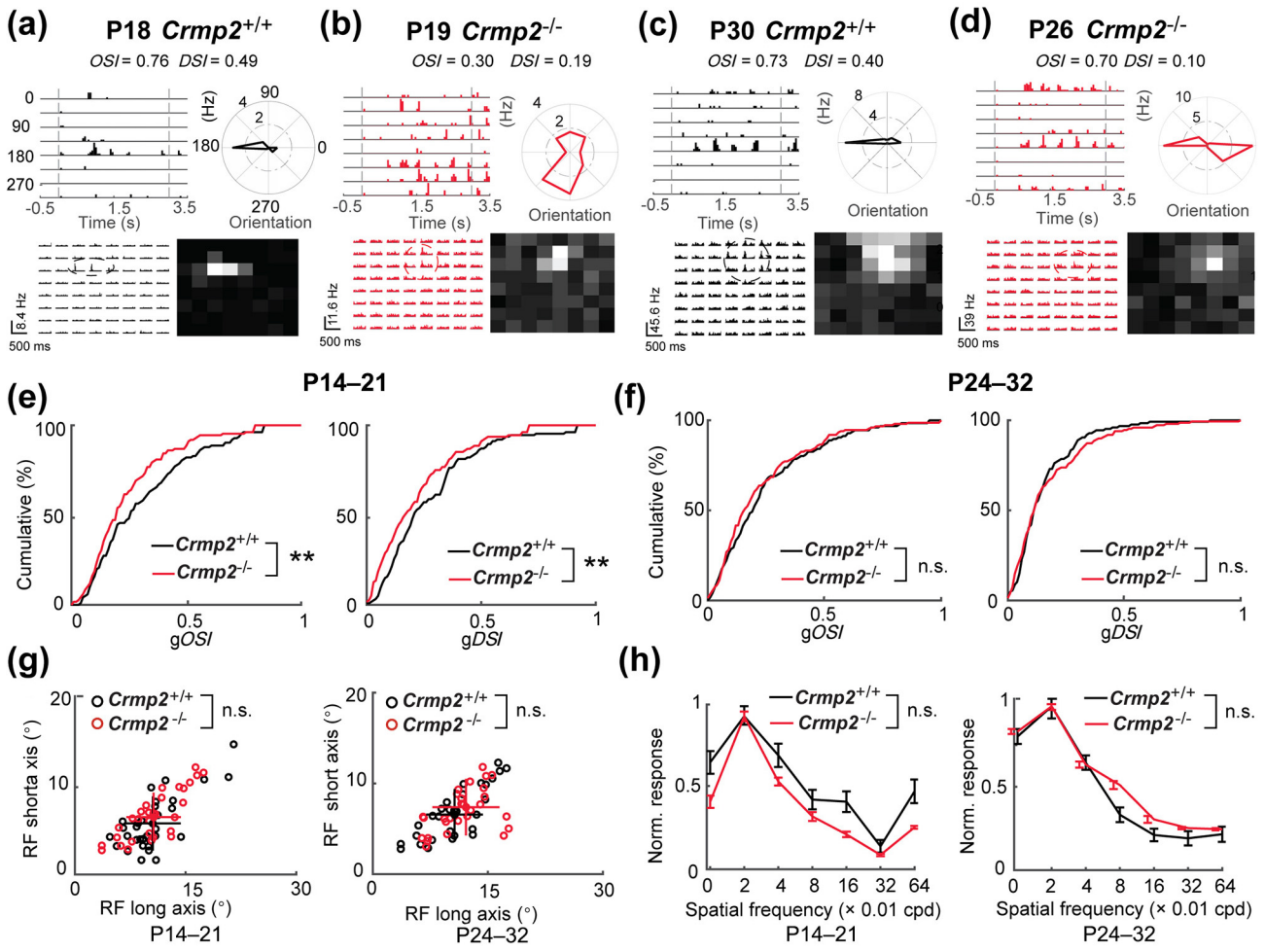

Fig. 1. Delayed maturation of orientation/direction tuning functions of CRMP2-deficient V1B cells. (a, b) Orientation tuning and RF property of an example V1B neuron in the *Crmp2*$^{+/+}$ mouse at P18 (a, black) or the *Crmp2*$^{-/-}$ mouse at P19 (b, red). Orientation/direction selectivity (*OSI* and *DSI*, respectively, top): peristimulus time histograms (PTSHs) and polar plots of spike rates evoked by drifting gratings at 8 different directions. Black vertical lines indicate the time of stimulation ON and OFF, respectively. RF (bottom): PTSHs of spike rates in response to a flashing bright square (~10°) at a discrete position in an 8 × 8 grid and the calculated spatial RF (outlined by the dashed line) based on spiking response variances. (c, d) Same as (a, b) except recording in the *Crmp2*$^{+/+}$ mouse at P30 (c) and the *Crmp2*$^{-/-}$mouse at P26 (d). (e) Cumulative percentage distributions of *gOSI* and *gDSI* strengths of recorded V1B neurons in the *Crmp2*$^{+/+}$mice (n = 117 cells, 5 mice) and *Crmp2*$^{-/-}$mice (n = 115 cells, 6 mice) at P14–21. *gOSI*: ** $P = 2.8 \times 10^{-3}$; *gDSI*: ** $P = 8.9 \times 10^{-3}$, Kolmogorov–Smirnov test. (f) Same as (e) except that measurements were performed in the two genotypes at P24–32 (n = 126 cells from 7 *Crmp2*$^{+/+}$ mice vs. n = 149 cells from 8 *Crmp2*$^{-/-}$mice). (g) Comparison of the RF size of V1B neurons in the two genotypes at P14–21 (left: n = 32 cells in *Crmp2*$^{+/+}$ mice vs. n = 31 cells in *Crmp2*$^{-/-}$mice) or at P24–32 (right: n = 32 cells in *Crmp2*$^{+/+}$mice group vs. n = 29 cells in *Crmp2*$^{-/-}$mice group). Each empty circle represents one cell. (h). Comparison of the spatial-frequency tuning curves of V1B neurons recorded in the two genotypes at P14–21 (left: n = 26 cells from 5 *Crmp2*$^{+/+}$ mice vs. n = 27 cells from 6 *Crmp2*$^{-/-}$mice) or at P24–32 (right: n = 53 cells from 7 *Crmp2*$^{+/+}$ mice vs. n = 42 cells from 8 *Crmp2*$^{-/-}$mice). Data in (h) are presented as mean ± standard error of the mean (SEM). n.s.: non-significant; *t*-test.

results indicate an earlier onset of experience-dependent OD plasticity in the *Crmp2*-KO mice.

The above different postnatal windows for the OD plasticity between the two genotypes were more evident by analyzing the *CBI* (Fig. 2e), a single parameter measuring an overall preference bias of 7-scale histograms for individual tested mice [8]. Moreover, we pooled the *CBI* value deviation (Δ*CBI*) between the normal reared (NR) and MD (Δ*CBI*) groups according to the MD beginning date, and the results clearly suggested that in the *Crmp2*-KO mice, the CP opened right after eye-opening and subsequently closed by P20, a time window that is much earlier than the normal one found in the control *Crmp2*$^{+/+}$ littermates (Fig. 2f). Taken together, by assaying the MD-induced OD plasticity of developing V1, we conclude that the *Crmp2* deficiency induces an aberrant CP with the precocious onset timing and shortened duration right after eye-opening in postnatal development.

3.3. An earlier emergence of the plasticity induction activity in V1B neurons of *Crmp2*$^{-/-}$mice

We previously elucidated that temporally coincident inputs from the two eyes to V1B neurons mediate the induction of OD plasticity and the coincident binocular activity is a hallmark of the CP [13]. Thus, we further confirmed the precocious onset of CP in the *Crmp2*-KO mice by measuring this hallmark activity in V1B neurons. Similar as our previous study [13], we conducted whole-cell recording of subthreshold postsynaptic potentials (PSPs) evoked by static gratings to contra- or ipsilateral eyes in V1B cells at P16–21 and P27–30, respectively, and then compared the calculated contra-ipsilateral PSP latency difference between the two stages (Fig. 3a, b). The pooled results show that the coincident binocular inputs in V1B neurons are emerged at P16–21 (before the normal CP) in the *Crmp2*-KO mice, while in the same

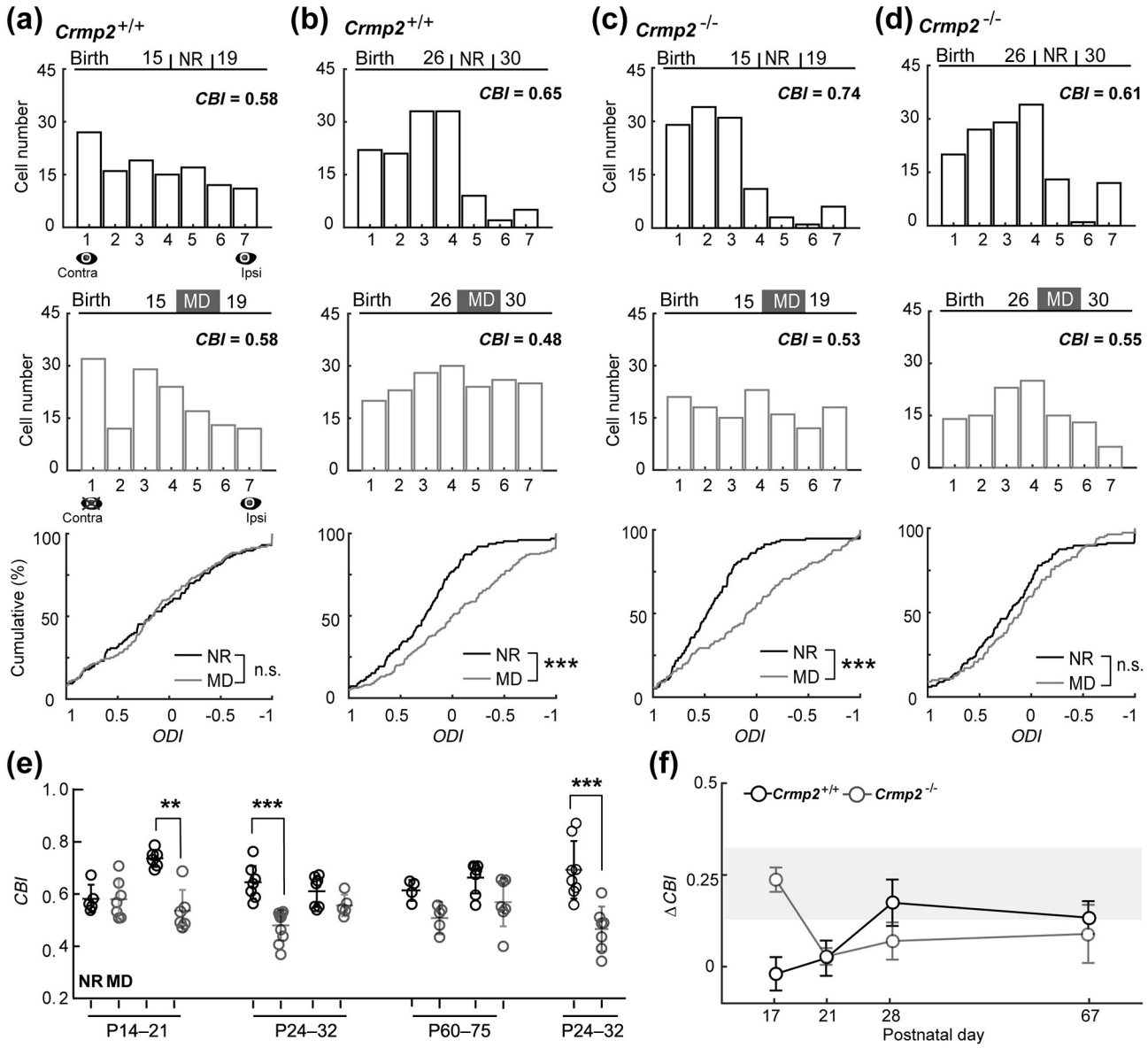

Fig. 2. Precocious onset of the CP for ocular dominance plasticity in the *Crmp2*$^{-/-}$mice. (a) 7-point histograms of *ODI*s of recorded V1B neurons in the *Crmp2*$^{+/+}$mice under NR conditions (top, n = 117 cells in 5 mice) and 4-day MD at P15 (middle, n = 139 cells in 7 mice), respectively. Bottom: the cumulative percentage distributions of *ODI*s of the same sets of V1B neurons. (b) Same as (a), except that NR and MD was performed in *Crmp2*$^{+/+}$ littermates at P26 (n = 125 cells in 7 mice for NR; n = 176 cells in 10 mice for MD; *** $P = 4.4 \times 10^{-7}$, Kolmogorov–Smirnov test). (c, d) Same as (a, b) except that the *Crmp2*$^{-/-}$mice were examined at P15 (c, n = 125 cells in 7 mice for NR; n = 176 cells in 10 mice under MD; ***, $P = 2.0 \times 10^{-8}$) or at P26 (d, n = 136 cells in 7 mice for NR; n = 111 cells in 5 mice for MD). (e) *CBI* values for individual tested animals shown in (a–d). Note that additional *CBI* values for the C57BL/6 WT mice are included as normal control (n = 120 cells in 8 mice for NR; n = 120 cells in 7 mice for MD). P14-21 *Crmp2*$^{-/-}$ group: ** $P = 2.2 \times 10^{-3}$; P24–32 *Crmp2*$^{+/+}$ group: *** $P = 1.0 \times 10^{-4}$; P24–32 WT group: *** $P = 6.2 \times 10^{-4}$, t-test. (f) Comparisons of the CP time window between the two genotypes, as indicated by the mean *CBI* value deviations between the NR and MD animals ($\Delta CBI = CBI_{NR} - CBI_{MD}$) when MD began at a day around P15, P17, P26, or P65. Shadowed area: mean ± SD of ΔCBI of the WT mice with the MD at P24–28. n.s.: non-significant.

period only asynchronized binocular inputs with an averaged ipsi-contra latency difference of ~40 ms were detected in the *Crmp2*$^{+/+}$ littermates or WT mice (Fig. 3c, d left). On the contrary, at P27–30 (within the normal CP), the binocular input coincidence could be detected in the *Crmp2*$^{+/+}$ littermates and WT mice but not in the *Crmp2*-KO mice any more (Fig. 3c, d right).

Moreover, additional comparisons of the onset latency of temporal receptive fields (tRFs) for contra- and ipsilateral eye inputs in some recorded V1B neurons (Fig. S2a–d online) also consistently suggested a precocious emergence of the binocular input coincidence in the CRMP2-deficient V1B neurons at P16–21, a time window much earlier than the normal CP (P27–30) observed in control *Crmp2*$^{+/+}$ littermates (Fig. S2e online).

Thus, the results of measuring the CP hallmark activity-coincident binocular inputs further consolidate the finding that the *Crmp2* deficiency induces a precocious onset of CP for experience-dependent visual cortical plasticity.

3.4. Crmp2 loss promotes the development of excitation-inhibition balance in vivo

Experience-dependent progressive establishment of E/I balanced sensory circuits is a key factor of controlling the CP onset and cortical function maturation during postnatal development [28]. We next addressed whether the E/I balance could be a cellular mechanism underlying the precocious CP induced by *Crmp2* defi-

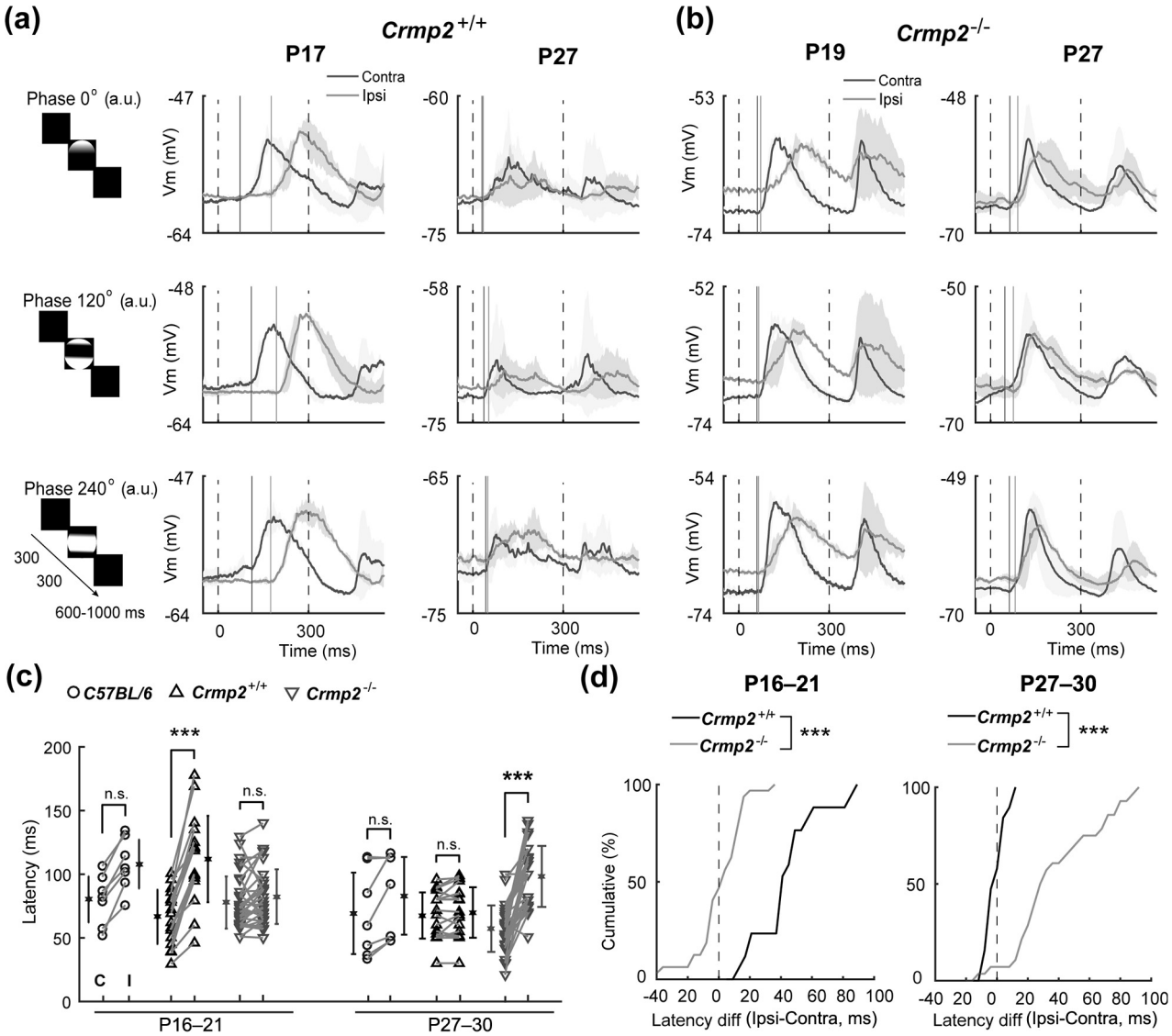

Fig. 3. Earlier emergence of binocular input coincidence in V1B neurons of *Crmp2*$^{-/-}$mice. (a) Traces of subthreshold PSPs evoked by static grating at 3 different spatial phases to the contra- (dark grey) or ipsi-lateral (light grey) eye in an example V1B neuron of the *Crmp2*$^{+/+}$ mouse at P17 and P27, respectively. Dashed vertical lines indicate the time of stimulation ON and OFF and solid lines indicate the PSP response latencies. Shading areas: PSP variation ranges. (b) Same as (a) except for a V1B cell recorded in a *Crmp2*$^{-/-}$mouse at P19 and P27, respectively. (c) Summary of the mean latency of evoked PSPs from experiments shown in (a) for the WT (circles) and two *Crmp2* genotypes (upward triangles and downward triangles) during two postnatal stages, respectively. Data connected with a line are from the same cell. C and I: contralateral or ipsilateral eye inputs. * $P = 0.05$, *** $P = 1.7 \times 10^{-5}$, *** $P = 3.8 \times 10^{-8}$; Wilcoxon signed-rank test. (d) Cumulative distribution of the Ipsi-Contra latency difference of V1B neurons in the two *Crmp2* genotypes at P16–21 for the *Crmp2*$^{+/+}$ (black) and *Crmp2*$^{-/-}$ (grey) mice at P16–21 ($n = 17$ cells from 8 *Crmp2*$^{+/+}$ mice vs. $n = 32$ cells from 16 *Crmp2*$^{-/-}$mice; *** $P = 1.6 \times 10^{-7}$, Kolmogorov-Smirnov test) and P27–30 ($n = 20$ cells from 10 *Crmp2*$^{+/+}$mice vs. $n = 28$ cells from 14 *Crmp2*$^{-/-}$mice; *** $P = 3.1 \times 10^{-9}$).

ciency, by conducting *in vivo* voltage-clamp whole-cell recording on V1B neurons to isolate excitatory and inhibitory input conductance (*Ge* and *Gi*) evoked by static gratings (Fig. 4a).

Similar to the previous study by Monier and colleagues [26], we correlatively plotted the magnitudes of isolated *Ge* and *Gi* of individual neurons from averaged postsynaptic currents (PSCs) for each stimulation trial, in which six static gratings were given to the contra- and ipsi-lateral eyes, respectively (Fig. 4b, c). The results showed that at P17–21, V1B neurons in the *Crmp2*-KO mice already had more balanced magnitudes between E/I inputs than those in the *Crmp2*$^{+/+}$ littermates, in which excitation was much larger than inhibition (Fig. 4b). However, at P27–29 the *Crmp2*$^{+/+}$ group developed similar extent of E/I balance as the *Crmp2*$^{-/-}$ mice (Fig. 4c). We also calculated the ratios of mean *Ge* and *Gi* peak amplitudes (the E/I ratio; Fig. 4d left) or mean *Ge* and *Gi* areas (Fig. 4d right) for either contra- or ipsi-lateral eye inputs in individual recorded V1B, respectively. The E/I ratio results clearly indicate that at P17–21, the *Crmp2*-KO group has a smaller value of the mean E/I ratio than the *Crmp2*$^{+/+}$ group, but at P27–29 there was no significant difference in the mean E/I ratio between two groups because of a developmental decrease of the E/I ratio in the *Crmp2*$^{+/+}$ group during this postnatal period. Thus, these *in vivo* synaptic conductance results directly support that the *Crmp2* loss promotes the development of E/I balanced cortical circuits shortly after eye-opening, which may account for the precocious onset of CP in the CRMP2-deficient V1.

3.5. Crmp2 loss-induced alterations of excitatory and inhibitory synaptic transmission

The above *Ge*/*Gi* results also indicated that CRMP2-deficient cortical circuits could have stronger GABAergic inhibitory transmission right after eye-opening. To directly elucidate this, we recorded miniature excitatory and inhibitory postsynaptic currents

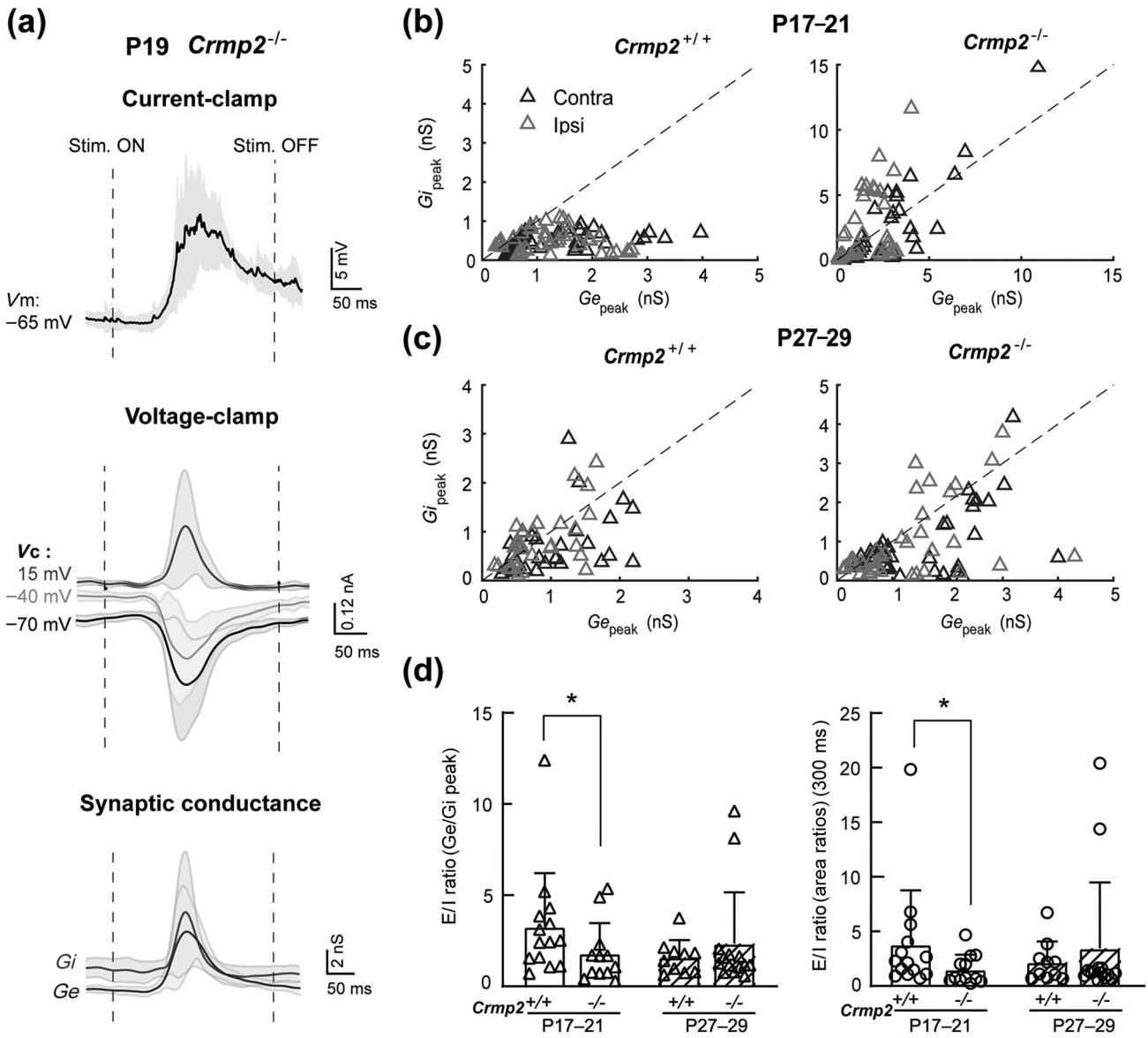

Fig. 4. Precocious onset of excitation-inhibition balance in visual responses in *Crmp2*$^{-/-}$ mice. (a) Traces of averaged postsynaptic potentials (top) as well as postsynaptic currents (middle) at clamped membrane potentials of −70, −40, and 15 mV, respectively, of an example CRMP2-deficient V1B neuron at P19, evoked by static gratings (at 3 spatial phases). *Bottom*: calculated *Ge* and *Gi*. Shading area: trial-to-trial SD. Vertical dash-lines: stimulation ON and OFF. (b) Correlative plots of *Ge* and *Gi* peak amplitudes for each trial of stimulation to either eye from *Crmp2*$^{+/+}$mice (left: n = 7 cells from 6 mice) or *Crmp2*$^{-/-}$littermates (right: n = 6 cells from 5 mice) at P17–21. (c) Same as (b) except for neurons recorded in *Crmp2*$^{+/+}$mice (left: n = 5 cells, 4 mice) or *Crmp2*$^{-/-}$littermates (right: n = 7 cells, 6 mice) at P27–29. (d) Comparisons of the mean E/I ratio (measured by the *Ge*/*Gi* peak or area ratios) between the two genotypes at P17–21 or P27–29. Each triangle or circle represents the mean E/I ratio for Contra- or Ipsi-lateral eye inputs in a recorded neuron. * P = 0.038 (left) and P = 0.018 (right), Mann-Whitney U-test.

(mEPSCs and mIPSPs) from layer II/III PCs located in the V1B zone in acute brain slices prepared from the *Crmp2*-KO or *Crmp2*$^{+/+}$ mice at two postnatal stages (P15–17 and P27–29), respectively. We found that at P15–17, CRMP2-deficient PCs indeed had substantially higher frequencies of mIPSCs but smaller amplitudes of mEPSCs, compared with than of *Crmp2*$^{+/+}$ control littermates (Fig. 5a, b). On the contrary, at P27–29 (within the normal CP) both frequencies and amplitudes of mIPSC events were not different between the two groups (Fig. 5d), whereas the frequency of mEPSCs in the CRMP2-deficient PCs became slightly higher than that of *Crmp2*$^{+/+}$ neurons (Fig. 5c). Thus, these results directly elucidate an accelerated functional maturation of cortical inhibitory transmission in the CRMP2-deficient V1 circuits shortly after eye-opening. However, the *Crmp2* loss did not induce any major changes of intrinsic excitability of layer II/III PCs at both stages (Fig. S3a online), although it had minor and variable effects on several basic membrane properties, such as input resistance, spike width, and after-hyperpolarization potential, at two different stages (Fig. S3c, d online).

It is generally known that functional maturation of cortical inhibitory parvalbumin-expressing (PV^{+}) cells, a major subtype of GABAergic interneuron (IN), is particularly critical for gating the CP opening [28]. The results of immuno-staining of PV expression and perineuronal net (PNN) structure, which are two molecular markers for more matured PV cells, indicated that the *Crmp2* loss resulted in the increases of PV cell densities and its PNN-enwrapping rates in the developing V1 at P14−20, which was more evident in the layers II/III and V/VI (Fig. S4a, c online). However, the numbers of GABA-immunostained INs in most cortical layers were slightly decreased in the *Crmp2*-KO mice, compared with that in

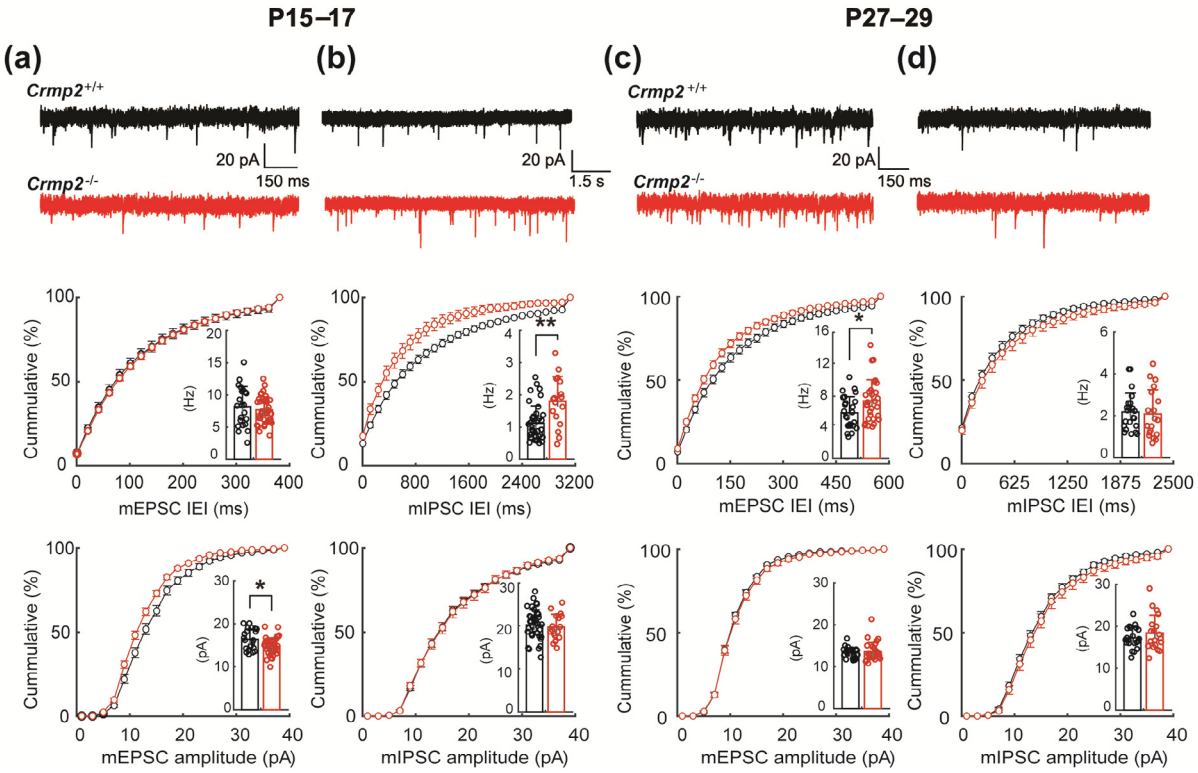

Fig. 5. Alternations of cortical excitatory and inhibitory transmission in *Crmp2*$^{-/-}$mice. (a) Top: mEPSC recording traces of a layer II/III PC in *Crmp2*$^{+/+}$ (black) and *Crmp2*$^{-/-}$ (red) mice at P15–17, respectively. Middle to bottom: cumulative distributions of inter-event intervals (IEIs) or amplitudes of mEPSC events in the two genotypes. Inserts: histogram bar plots of the mean frequency or amplitude of mEPSCs. Each circle represents one recorded neuron (n = 22 cells from 3 *Crmp2*$^{+/+}$ mice vs. n = 38 cells from 4 *Crmp2*$^{-/-}$ mice; * P = 0.01, t-test. (b) Same as (a) except mIPSCs were measured in the two genotypes at P15–17 (n = 39 cells from 6 *Crmp2*$^{+/+}$mice vs. n = 17 cells from 3 *Crmp2*$^{-/-}$mice; *** $P = 3.7 \times 10^{-4}$, t-test). (c, d) Same as (a, b) except that the two genotypes were examined at P27–29. mEPSCs: n = 25 cells from 3 *Crmp2*$^{+/+}$ mice vs. n = 29 cells from 4 *Crmp2*$^{-/-}$ mice; * P = 0.02. mIPSCs: n = 22 cells from 3 *Crmp2*$^{+/+}$ mice vs. n = 19 cells from 3 *Crmp2*$^{-/-}$ mice. Data are shown as mean ± SEM.

the control littermates, at both P14–20 and P25–31 stages (Fig. S4b, d online). We thus deduced that the stronger inhibition observed in both *in vivo* and slice recordings in the CRMP2-deficient V1 circuits could be attributed to accelerated pace of molecular maturation of PV cells shortly after eye-opening.

3.6. Deteriorated binocular depth perception in adult *Crmp2*$^{-/-}$mice

Normal experience-dependent CP plasticity of developing V1 is known to be extremely important for the formation of binocular vision functions [9]. Based on observations of the delayed orientation/direction tuning maturation and the precocious CP in the CRMP2-deficient V1 within the first week after eye-opening, we deduced that these development defects are very likely to induce an aberrant OD plasticity and then lead to persistent deficits in binocular vision functions. To directly test this idea, we performed the classical visual-cliff behavioral tests [29], including the depth exploration task (Fig. 6a) and the depth descent test (Fig. 6d), in adult mice (7.5–8 weeks old).

In the depth exploration test, we first calculated the $E_{\text{-score}}$ (the ratio of the summed actual time and the expected time in the separated zones) for the deep and shallow zones during the first 3 min of animal's spontaneous exploration on the arena, respectively, and then assessed their preference to which zone with the *EBI*. The *EBI* values of 1 and −1 represented the complete bias to the shallow zone and the deep zone, respectively. Different patterns of animal's exploration trajectories were observed between the *Crmp2*-KO mouse and the *Crmp2*$^{+/+}$ control littermate (Fig. 6b and Movies S1, S2 online). The pooled *EBI* values for tested individual animals further suggested that unlike the adult control mice, exploration behaviors of the *Crmp2*-KO mice did not exhibit the same strong preference to the shallow zone (Fig. 6c left). The extent of deteriorated depth perception in adult *Crmp2*-KO mice was similar to that of the WT mice which were rendered amblyopic by a long-term MD (LTMD) for 1 month (starting from the CP onset P21) (Fig. 6c right, Fig. S5b, and Movies S3, S4 online).

Moreover, the *Crmp2*$^{+/+}$or WT mice with a whisker trimming still displayed similar extents of behavioral preference as those with intact whiskers for each genotype (Fig. 6c, W-Trim groups; Fig. S5a, b online), suggesting that tactile inputs had little influence on animals' performance in this task. It was worth noting that the whisk-trimmed *Crmp2*-KO mice had even worse performance, with a mean *EBI* value that was close to zero (Fig. 6c). This could possibly be attributed to complex developmental defects associated with somatosensory and other sensory circuits. The whisker trimming appeared not to significantly change the anxiety level of animals (as indicated by the $E_{\text{-score}}$ index (*EI*) in the center zone), but slightly decreased the locomotion velocity only in the *Crmp2*$^{+/+}$mice (Fig. S5c, d online). Thus, the results of whisker-trimming experiments suggest that in the depth exploration task, mice could mainly rely on visual cues rather than tactile information for perceiving different depths and further support the conclusion that the *Crmp2*-KO mice have a deteriorated depth perception in adulthood.

We also characterized the retreating, freezing, and grooming behaviors of animals in the deep, center and, shallow zones, respectively, and found that proportions of the time of exhibiting above three behaviors were consistently low in both *Crmp2*-KO and control littermates (Fig. S5e online), implicating comparably low levels of anxiety. However, we noted that the *Crmp2*-KO mice had substantially fewer retreating behaviors in the center zone, a

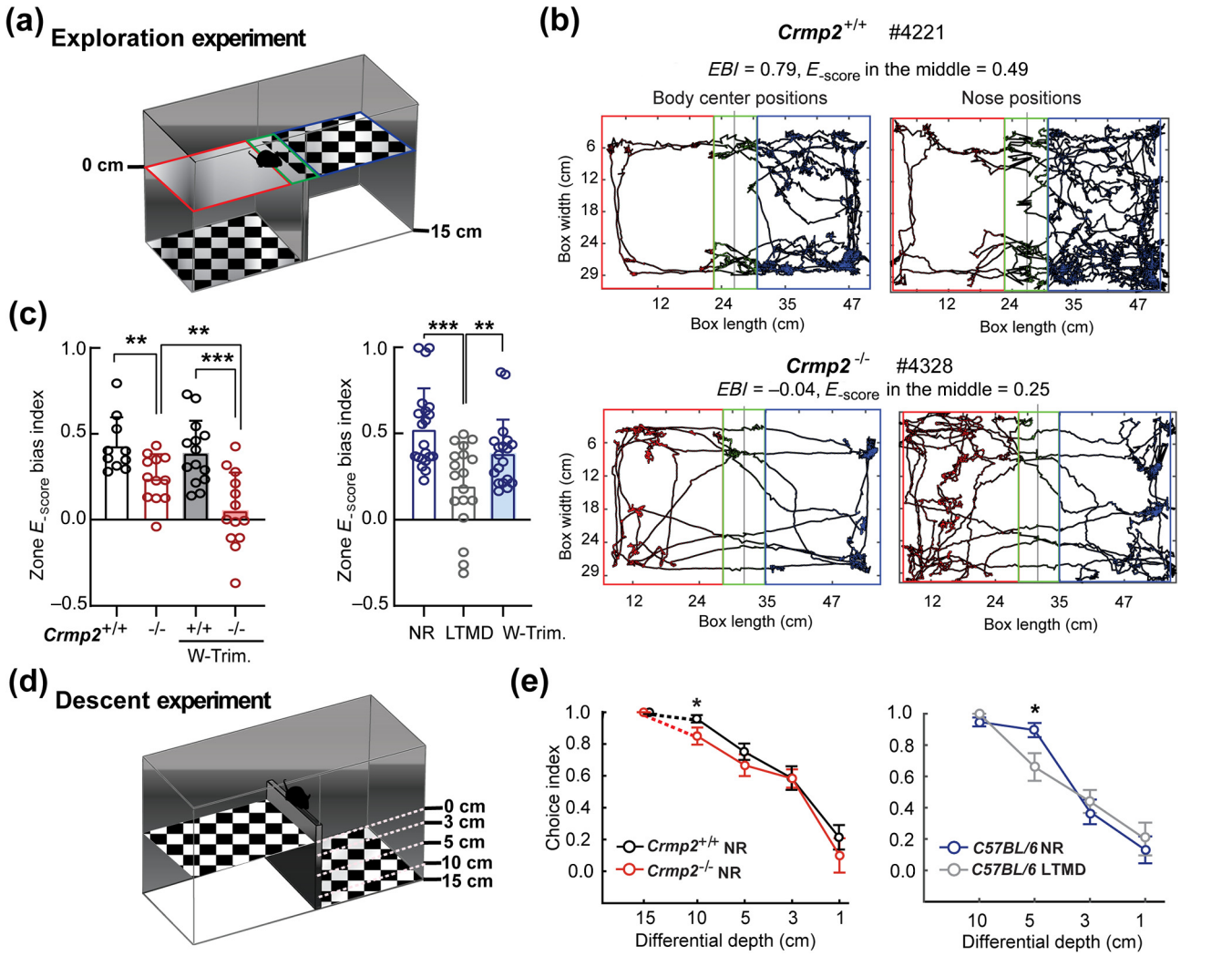

Fig. 6. Deteriorated depth perception in adult *Crmp2*$^{-/-}$ mice. (a) Experimental apparatus and design for the depth exploration test. The shallow, deep, and central zones are indicted by blue, red, and green rectangles, respectively. (b) Trajectories of spontaneous exploration of an adult *Crmp2*$^{+/+}$ (#4221) and *Crmp2*$^{-/-}$mouse (#4328), respectively, within the first 3 min in exploration, on the basis of analyzing positions of the body center (left) or the nose (right). (c) Left: comparison of the zone *EBI* in the exploration task between the two *Crmp2* genotypes with whisker intact (n = 10 *Crmp2*$^{+/+}$ mice vs. n = 12 *Crmp2*$^{-/-}$ mice; ** $P = 3.9 \times 10^{-3}$) or trimmed (W-Trim, n = 13 *Crmp2*$^{-/-}$mice *vs.* n = 14 *Crmp2*$^{+/+}$ mice, *** $P = 1.2 \times 10^{-4}$; or vs. the *Crmp2*$^{-/-}$ with intact whiskers group, ** $P = 9.4 \times 10^{-3}$). *Right*: comparisons among the WT mouse groups with normal rearing (NR), long-term MD or whisker trimming (n = 18 LTMD mice vs. n = 21 NR mice, *** $P = 7.0 \times 10^{-5}$; or vs. n = 19 W-Trim mice, ** $P = 7.6 \times 10^{-3}$). (d) Experimental apparatus and design for the depth descent task. The depth differences varied 1, 3, 5, 10, or 15 cm randomly in the experiments. (e) Comparison of the choice index (CI) for the descent tasks between the two *Crmp2* genotypes (left: tests of depth difference ≤ 10 cm, n = 29 *Crmp2*$^{+/+}$mice vs. n = 24 *Crmp2*$^{-/-}$ mice, * P = 0.03). Note that only 12 *Crmp2*$^{+/+}$and 12 *Crmp2*$^{-/-}$ mice were subjected to tests at 15 cm depth difference. Comparison between the WT mice with NR and LTMD (right: n = 23 NR mice vs. n = 20 LTMD mice, * P = 0.01). Data are shown as mean ± SEM. All P values were calculated by t-test.

behavior that could be involved with assessing visual cues along the edge of shallow and deep zones (Fig. S5e online). It could be possibly caused by the deteriorated visual perception of depth edge in the *Crmp2*-KO mice.

Finally, the same animal groups were trained to make a forced choice of jumping from a narrow platform to either shallow or deep board, along with setting various height differences of 1, 3, 5, 10, or 15 cm between the two boards (set in a pseudorandom sequence in trials, Fig. 6d). In the depth descent task, the choice index (CI) was calculated for each tested depth difference to evaluate the perceptual threshold. The results indicated that the *Crmp2*-KO mice and the LTMD mice showed a significantly degraded performance at a height difference of 10 cm and 5 cm, respectively, when compared with the control *Crmp2*$^{+/+}$ littermates and the normally-reared WT mice (Fig. 6e right). It indicates that the *Crmp2*-KO mice possess the severest deterioration in binocular perception of depths among the tested four animal groups.

Taken together, the results of the classical visual-cliff behavioral tests support our idea that the *Crmp2* loss-induced dysregulations of the CP plasticity in developing V1 leads to a persistent deterioration of binocular depth perception in adulthood.

4. Discussion and conclusion

In this study, by examining the classical experience-dependent OD plasticity of developing mouse V1, we revealed a new role of schizophrenia-risk gene *Crmp2* in regulating the timing of CP for neuronal circuit refinement and maturation during postnatal development. The *Crmp2* loss induced a precocious onset and closure of CP for the OD plasticity, a result that was mainly caused by the accelerated maturation of cortical inhibitory transmission along with the resultant earlier establishment of E/I balance in the mouse early juvenile stage (P15–21, a period shortly after

eye-opening). Such an aberrant CP plasticity in the *Crmp2*-KO mice led to a deterioration of depth perception in adulthood. Thus, our findings suggest that a dysregulation of the CP associated with the *Crmp2* deficiency is a cause of the impaired sensory function observed in the later life of mice with schizophrenia-like behaviors.

4.1. Roles of CRMP2 in regulating circuit development and plasticity

The gene *Crmp2* is ubiquitously expressed in the brain, with a substantially higher level in the early development [10,11]. CRMP2 was originally identified as a signaling molecule that was essential for growth cone collapse of dorsal root ganglion neurons in response to semaphorin-3A [2], and it has also been reported to play active roles in several developmental processes including axon-dendrite specification, axonal extension and regeneration, as well as dendritic field organization [12]. Its primary downstream effectors are the actin, tubulin, and other cytoskeletal proteins, thus a CRMP2 deficiency could often lead to severe deficits in neuronal morphological development and migration during the early development, which has been thought as possible etiopathogenesis for schizophrenia [29,30].

In addition to its well-established roles in neural structure development, our current study has revealed a new role of CRMP2 in controlling the timing of postnatal CPs for early experience-dependent refinement and function maturation of sensory cortical circuits. We here demonstrated that the *Crmp2* loss could induce a precocious onset of CP for OD plasticity in developing V1 shortly after the eye opening. This is accompanied with a delayed maturation of orientation/direction tuning functions in the CRMP2-deficient V1 neurons. However, these tuning properties were restored to normal functional levels at the later postnatal stages. It implies that the tuning function defects could possibly be attributed to delayed circuit formation associated with the *Crmp2* loss before the eye-opening, because most basic visual tuning functions of V1 neurons are known to be formed before eye-opening and are slightly malleable to experience alternations [31,32]. In contrast, experience-dependent OD plasticity during the CP is critical for the formation and maturation of binocular stereo vision or depth perception, severing as a mechanism for response strength and spatiotemporal feature matching (e.g., orientations, timing, and RF structures) matching between two eyes [13,33–36]. Thus, dysregulation of the CP, e.g., the precocious onset and reduced length of the CP induced by the *Crmp2* deficiency, could cause an aberrant CP plasticity of developing V1B circuits and then lead to a persistent impairment in binocular vision functions in the adult stage. This persistent impairment is evident in the tested *Crmp2*-KO mice with the classic visual cliff tasks for depth perception (Fig. 6). Interestingly, two other schizophrenia risk-genes disrupted in schizophrenia 1 (*DISC1*) and neuregulin-1 (*Nrg1*)/erb-b2 receptor tyrosine kinase 4 (*ErbB4*) were also found to be involved in regulating the CP plasticity of V1 [37–40]. Because that schizophrenia is generally regarded as a neurodevelopmental disorder resulted from neural development deficits primarily during defined postnatal temporal windows [4,41], these findings of schizophrenia risk-gene's function in regulating developmental circuit plasticity can shed new insights on its synaptic pathologies.

A similar precocious onset of CP plasticity in the developing V1 was also observed in the transgenic mice with constitutive loss of a Rett-syndrome gene methyl-CpG binding protein 2 (*Mecp2*) right after eye-opening [42]. On the contrary, we previously found that conditional deletion of *Mecp2* in inhibitory PV cells, but not in inhibitory somatostatin (SOM)-expressing cells or excitatory PCs, resulted in the absence of CP plasticity in the developing mouse V1 [43]. These MeCP2 studies indicate that cell subtype- or germ line-specific loss of a critical development-related gene could generally have different forms of dysregulation of the CP for early experience-dependent cortical plasticity. However, it remains to be examined how specific deletion of *Crmp2* in different subtypes of neuron affects functional development and plasticity of neural circuits.

Our results of assaying MD-induced OD plasticity also suggest that the duration of CP was also shortened in the *Crmp2*-KO mice, implicating a possible earlier closure of the CP. However, it is still unclear what specific cellular or molecular factors function as brakes on critical period plasticity [9,44]. There is evidence for suggesting several potential explanations, such as the continuous elevation of inhibition [45], epigenetic modification [46], neuromodulatory desensitization [47,48], or developmental maturation of PNN structures [49,50]. Developmental maturation of PNNs of the extracellular matrix could potentially cast a persistent structural protection on synapses from experience-induced modifications. However, our results of unaffected maturation of PNN structures in CRMP2-deficient V1 circuits may imply that PNN maturation is not a factor leading to an earlier closure of CP in the *Crmp2*-KO mice.

4.2. Implication of CRMP2 in regulating cortical inhibition maturation

In individual principal PCs, magnitudes of synaptic inhibition are proportionally augmented along with excitation level increasing [26]. Such balanced E/I inputs are important for neuronal function operations such as visual cortical feature tunings [51], gating CP plasticity [52], and information encoding [53]. An approach to restore the E/I balanced circuits has emerged as a new therapeutic intervention to certain pathological alterations of schizophrenia [54]. In the present study, our *in vivo* E/I conductance measurement results indicated that visually evoked excitatory inputs overwhelmed inhibitory inputs in V1B principal neuron right after eye-opening (P16−21), while balanced E/I inputs was first observed within the normal CP (Fig. 2e, f and Fig. 3c) mainly due to a gradual increase of cortical inhibitory transmission (Fig. 4b, d). However, we found that in the CRMP2-deficient cortical circuit, balanced E/I inputs appeared precociously right after eye-opening (Fig. 4a, b, d). Stronger inhibitory transmission was consistently observed in the CRMP2-deficient circuit within the same period (Fig. 5b). These two observations directly suggest that the *Crmp2* loss could preferentially accelerate the maturation process of cortical inhibitory transmission in very early postnatal development, which leads to precocious onsets of the E/I balance and the CP plasticity in developing V1 shortly after eye-opening.

Similarly the acceleration of inhibitory transmission maturation was also found in other transgenic mice exhibiting a precocious CP, for examples those with an overexpression of neural trophic factors [27] or the homeodomain protein orthodenticle homeobox 2 (Otx2) [55], those with a deletion of a cell adhesion molecule polysialic acid [56] or a transcription modulator MECP2 [42], and those treated by the γ-aminobutyric acid (GABA) A receptor modulator benzodiazepines [57]. Our previous study of systemic characterization of E/I synaptic transmission changes in mouse V1 circuits within a specific period from eye-opening to the CP onset uncovered that PV cell-mediated inhibition was selectively augmented, accompanied by gradual reduction of the inhibition mediated by another major subtype SOM-expressing interneurons [58]. At the molecular level, our current results of neuronal PNN structure staining also consistently suggest a similar maturation of cortical PV cells in the control mice, but a substantially faster pace in the *Crmp2*-knockout mice (Fig. S4 online). Thus, we deduce that the accelerated maturation of cortical PV cells following the *Crmp2* loss is one of the major reasons for precocious onsets of the E/I balance and the CP plasticity in developing V1. This deduction agrees with the general idea of gating the CP onset by cortical inhibitory PV cells [28].

It is still largely unknown how CRMP2-related molecular signaling regulates synaptic functional maturation and plasticity during the postnatal development. Previous studies implicated that CRMP2 could affect glutamatergic transmission possibly through its modulation on the N-type Ca^{2+} channel [59,60]. It may account for the observed alteration of excitatory transmission in the CRMP2-deficient visual cortical circuits (Fig. 5a, c). Moreover, the presynaptic CRMP2-Cav2.2 interaction was reported to relate to the glycogen synthase kinase (GSK)-3β regulatory pathway [61]. It is of interest to clarify the molecular mechanism by which the CRMP2 deficiency induces dysregulation of synaptic function and plasticity.

4.3. Impaired binocular vision function in the schizophrenia

Another significant finding of our present study is that the precocious CP plasticity of developing V1 in the *Crmp2*-KO mice leads to a deteriorated function of binocular depth perception in later life. Our results indicate that the adult *Crmp2*-KO mice showed apparent impaired performance of depth discrimination in both classical visual cliff tests – the depth exploration task and the depth descent task (Fig. 6 and Fig. S5 online). The behavioral impairments are mainly due to a poor binocular vision function in the *Crmp2*-KO mice, because whisker-trimmed mice exhibited comparable levels of performance as the whisker-intact animals in the depth exploration task. Given the finding of aberrantly precocious CP plasticity of developing V1 in the *Crmp2*-KO mice, these behavioral test results supports the idea that development of binocular vision relies on normal experience-dependent CP plasticity [13,33]. Interestingly, several human-subject studies reported that schizophrenia patients consistently had degraded functions in binocular depth perception or stereo vision [62–64]. It has been thought that the binocular vision deficit in patients could be a reason for their apparently poor performance commonly seen in several daily tasks, such as pouring water into a glass, threading a needle, keeping balance and so on [62], and it may also contribute to the dyspraxia in many patients [62]. Although our animal study concluded that the aberrant OD plasticity during the precocious CP induced by deficiency of schizophrenia-risk gene *Crmp2* may account for impaired depth perception in adulthood, this notion needs to be further verified in the research of human vison development, particularly in schizophrenia patients. Moreover, the postnatal CPs for experience-dependent neuronal connection refinements are prevalent in the process of functional maturation of many other sensory cortices (e.g., the auditory or somatosensory cortex, [65,66]), the cerebellum [67], and the high-level cortex for social or language function [68]. We may speculate that the *Crmp2* deficiency is very likely to induce similar dysregulations of the CP plasticity in the above-mentioned brain circuits, which needs to be examined in future studies.

In conclusion, given that the gene *Crmp2* is one of the key schizophrenia-risk genes, our animal study has revealed that a *Crmp2* deficiency induces a precocious onset of the postnatal CP for experience-dependent refinement of circuit connections in the developing sensory cortex. The latter dysregulation of CP plasticity could lead to deteriorated function of binocular depth perception in the later life. Thus, our findings provide a developmental circuit plasticity mechanism that may underlie abnormal sensory functions in neurodevelopmental diseases such as schizophrenia.

Conflict of interest

The authors declare that they have no conflict of interest.

Acknowledgments

This work was supported by the National Natural Science Foundation of China (32071025, 31921002, and 31730108), the Beijing Municipal Science & Technology Commission (Z181100001518001), the Interdisciplinary Research Fund of Beijing Normal University, and the Strategic Priority Research Program and Innovation Program of the Chinese Academy of Sciences (XDB32020100).

Author contributions

Xiaohui Zhang, Zhiheng Xu, and Yuan Zhang conceived the research and designed the experiments. Yuang Zhang performed the *in vivo* recording and data analysis. Li Yao and Xiang Li conducted slice electrophysiology and immunostaining experiments, respectively. Meizhen Meng, Yuan Zhang, and Ziwei Shang performed the mouse behavioral tests. Qin Wang, Jiaying Xiao, and Xiang Gu prepared the transgenic mice. Xiaohui Zhang and Yuan Zhang wrote the manuscript with the inputs from all other authors.

Appendix A. Supplementary materials

Supplementary materials to this article can be found online at https://doi.org/10.1016/j.scib.2021.02.011.

References

[1] Keshavan MS, Giedd J, Lau JYF, et al. Changes in the adolescent brain and the pathophysiology of psychotic disorders. Lancet Psychiatry 2014;1:549–58.
[2] Goshima Y, Nakamura F, Strittmatter P, et al. Collapsin-induced growth cone collapse mediated by an intracellular protein related to UNC-33. Nature 1995;376:509–14.
[3] Johnston-Wilson NL, Sims CD, Hofmann J-P, et al. Disease-specific alterations in frontal cortex brain proteins in schizophrenia, bipolar disorder, and major depressive disorder. Mol Psychiatry 2000;5:142–9.
[4] Tabarés-Seisdedos R, Rubenstein JLR. Chromosome 8p as a potential hub for developmental neuropsychiatric disorders: implications for schizophrenia, autism and cancer. Mol Psychiatry 2009;14:563–89.
[5] Bretin S, Reibel S, Charrier E, et al. Differential expression of CRMP1, CRMP2A, CRMP2B, and CRMP5 in axons or dendrites of distinct neurons in the mouse brain. J Comp Neurol 2005;486:1–17.
[6] Ip JPK, Fu AKY, Ip NY. CRMP2: functional roles in neural development and therapeutic potential in neurological diseases. Neuroscience 2014;20:589–98.
[7] Zhang H, Kang E, Wang Y, et al. Brain-specific *Crmp2* deletion leads to neuronal development deficits and behavioural impairments in mice. Nat Commun 2016;7:11773.
[8] Gordon JA, Stryker MP. Experience-dependent plasticity of binocular responses in the primary visual cortex of the mouse. J Neurosci 1996;16:3274–86.
[9] Espinosa JS, Stryker M. Development and plasticity of the primary visual cortex. Neuron 2012;75:230–49.
[10] Cnops L, Van de Plas B, Arckens L. Age-dependent expression of collapsin response mediator proteins (CRMPs) in cat visual cortex. Eur J Neurosci 2004;19:2345–51.
[11] Cnops L, Hu T-T, Burnat K, et al. Age-dependent alterations in CRMP2 and CRMP4 protein expression profiles in cat visual cortex. Brain Res 2006;1088:109–19.
[12] Hensley K, Venkova K, Christov A, et al. Collapsin response mediator protein-2: an emerging pathologic feature and therapeutic target for neurodisease indications. Mol Neurobiol 2011;43:180–91.
[13] Chen X-j, Rasch MJ, Chen G, et al. Binocular input coincidence mediates critical period plasticity in the mouse primary visual cortex. J Neurosci 2014;34:2940–55.
[14] Gan J, Weng SM, Pernia-Andrade AJ, et al. Phase-locked inhibition, but not excitation, underlies hippocampal ripple oscillations in awake mice *in vivo*. Neuron 2017;93:308–14.
[15] Liu B-H, Li P, Sun YJ, et al. Intervening inhibition underlies simple-cell receptive field structure in visual cortex. Nat Neurosci 2010;13:89–96.
[16] Wang Y, Liu Y-Z, Wang S-y, et al. *In vivo* whole-cell recording with high success rate in anaesthetized and awake mammalian brains. Mol Brain 2016;9:86.
[17] Zhang S-y, Xu M, Miao Q-l, et al. Endocannabinoid-dependent homeostatic regulation of inhibitory synapses by miniature excitatory synaptic activities. J Neurosci 2009;29:13222–31.
[18] Ye Q, Miao Q-L. Experience-dependent development of perineuronal nets and chondroitin sulfate proteoglycan receptors in mouse visual cortex. Matrix Biol 2013;32:352–63.

[19] Ben-Shaul Y. OptiMouse: a comprehensive open source program for reliable detection and analysis of mouse body and nose positions. BMC Biol 2017;15:41.
[20] Ringach DL, Shapley RM, Hawken MJ. Orientation selectivity in macaque V1: diversity and laminar dependence. J Neurosci 2002;22:5639–51.
[21] Inayat S, Barchini J, Chen H, et al. Neurons in the most superficial lamina of the mouse superior colliculus are highly selective for stimulus direction. J Neurosci 2015;35:7992–8003.
[22] Mazer JA, Vinje WE, McDermott J, et al. Spatial frequency and orientation tuning dynamics in area V1. Proc Natl Acad Sci USA 2002;99:1645–50.
[23] Wehr M, Zador AM. Balanced inhibition underlies tuning and sharpens spike timing in auditory cortex. Nature 2003;426:442–6.
[24] Ye C-q, Poo M-m, Dan Y, et al. Synaptic mechanisms of direction selectivity in primary auditory cortex. J Neurosci 2010;30:1861–8.
[25] Pernia-Andrade AJ, Goswami SP, Stickler Y, et al. A deconvolution-based method with high sensitivity and temporal resolution for detection of spontaneous synaptic currents *in vitro* and *in vivo*. Biophys J 2012;103:1429–39.
[26] Monier C, Fournier J, Frégnac Y. *In vitro* and *in vivo* measures of evoked excitatory and inhibitory conductance dynamics in sensory cortices. J Neurosci Methods 2008;169:323–65.
[27] Hanover JL, Huang ZJ, Tonegawa S, et al. Brain-derived neurotrophic factor overexpression induces precocious critical period in mouse visual cortex. J Neurosci 1999;19:RC40.
[28] Hensch TK. Critical period plasticity in local cortical circuits. Nat Rev Neurosci 2005;6:877–88.
[29] Fukata Y, Itoh TJ, Kimura T, et al. CRMP-2 binds to tubulin heterodimers to promote microtubule assembly. Nat Cell Biol 2002;4:583–91.
[30] Marchisella F, Coffey ET, Hollos P. Microtubule and microtubule associated protein anomalies in psychiatric disease. Cytoskeleton 2016;73:596–611.
[31] Ko Ho, Cossell L, Baragli C, et al. The emergence of functional microcircuits in visual cortex. Nature 2013;496:96–100.
[32] Ko H, Mrsic-Flogel TD, Hofer SB. Emergence of feature-specific connectivity in cortical microcircuits in the absence of visual experience. J Neurosci 2014;34:9812–6.
[33] Wang B-S, Sarnaik R, Cang J. Critical period plasticity matches binocular orientation preference in the visual cortex. Neuron 2010;65:246–56.
[34] Wang B-S, Feng L, Liu M, et al. Environmental enrichment rescues binocular matching of orientation preference in mice that have a precocious critical period. Neuron 2013;80:198–209.
[35] Salinas KJ, Figueroa Velez DX, Zeitoun JH, et al. Contralateral bias of high spatial frequency tuning and cardinal direction selectivity in mouse visual cortex. J Neurosci 2017;37:10125–38.
[36] Smith SL, Trachtenberg JT. Experience-dependent binocular competition in the visual cortex begins at eye opening. Nat Neurosci 2007;10:370–5.
[37] Blackwood DHR, Fordyce A, Walker MT, et al. Schizophrenia and affective disorders—cosegregation with a translocation at chromosome 1q42 that directly disrupts brain-expressed genes: clinical and P300 findings in a family. Am J Hum Genet 2001;69:428–33.
[38] Millar JK, Wilson-Annan JC, Anderson S, et al. Disruption of two novel genes by a translocation co-segregating with schizophrenia. Hum Mol Genet 2000;9:1415–23.
[39] Mei L, Nave K-A. Neuregulin-ERBB signaling in the nervous system and neuropsychiatric diseases. Neuron 2014;83:27–49.
[40] Harrison PJ, Weinberger DR. Schizophrenia genes, gene expression, and neuropathology: on the matter of their convergence. Mol Psychiatry 2005;10:40–68.
[41] Lewis DA, Levitt P. Schizophrenia as a disorder of neurodevelopment. Annu Rev Neurosci 2002;25:409–32.
[42] Krishnan K, Wang B-S, Lu J, et al. MeCP2 regulates the timing of critical period plasticity that shapes functional connectivity in primary visual cortex. Proc Natl Acad Sci USA 2015;112:E4782–91.
[43] He L-J, Liu N, Cheng T-L, et al. Conditional deletion of *Mecp2* in parvalbumin-expressing GABAergic cells results in the absence of critical period plasticity. Nat Commun 2014;5:5036.
[44] Bavelier D, Levi DM, Li RW, et al. Removing brakes on adult brain plasticity: from molecular to behavioral interventions. J Neurosci 2010;30:14964–71.
[45] Sale A, Berardi N, Spolidoro M, et al. GABAergic inhibition in visual cortical plasticity. Front Cell Neurosci 2010;4:10.
[46] Putignano E, Lonetti G, Cancedda L, et al. Developmental downregulation of histone posttranslational modifications regulates visual cortical plasticity. Neuron 2007;53:747–59.
[47] Morishita H, Miwa JM, Heintz N, et al. Lynx1, a cholinergic brake, limits plasticity in adult visual cortex. Science 2010;330:1238–40.
[48] Vetencourt JFM, Sale A, Viegi A, et al. The antidepressant fluoxetine restores plasticity in the adult visual cortex. Science 2008;320:385–8.
[49] Pizzorusso T, Medini P, Berardi N, et al. Reactivation of ocular dominance plasticity in the adult visual cortex. Science 2002;298:1248–51.
[50] McGee AW, Yang Y, Fischer QS, et al. Neuroscience: experience-driven plasticity of visual cortex limited by myelin and nogo receptor. Science 2005;309:2222–6.
[51] Liu B-H, Li Y-T, Ma W-P, et al. Broad inhibition sharpens orientation selectivity by expanding input dynamic range in mouse simple cells. Neuron 2011;71:542–54.
[52] Kuhlman SJ, Olivas ND, Tring E, et al. A disinhibitory microcircuit initiates critical-period plasticity in the visual cortex. Nature 2013;501:543–6.
[53] Fries P. Neuronal gamma-band synchronization as a fundamental process in cortical computation. Annu Rev Neurosci 2009;32:209–24.
[54] Gonzalez-Burgos G, Cho RY, Lewis DA. Alterations in cortical network oscillations and parvalbumin neurons in schizophrenia. Biol Psychiatry 2015;77:1031–40.
[55] Sugiyama S, Di Nardo AA, Aizawa S, et al. Experience-dependent transfer of Otx2 homeoprotein into the visual cortex activates postnatal plasticity. Cell 2008;134:508–20.
[56] Di Cristo G, Chattopadhyaya B, Kuhlman SJ, et al. Activity-dependent PSA expression regulates inhibitory maturation and onset of critical period plasticity. Nat Neurosci 2007;10:1569–77.
[57] Fagiolini M, Hensch TK. Inhibitory threshold for critical-period activation in primary visual cortex. Nature 2000;404:183–6.
[58] Miao Q, Yao Li, Rasch MJ, et al. Selective maturation of temporal dynamics of intracortical excitatory transmission at the critical period onset. Cell Rep 2016;16:1677–89.
[59] Brittain JM, Piekarz AD, Wang Y, et al. An atypical role for collapsin response mediator protein 2 (CRMP-2) in neurotransmitter release via interaction with presynaptic voltage-gated calcium channels. J Biol Chem 2009;284:31375–90.
[60] Chi XX, Schmutzler BS, Brittain JM, et al. Regulation of N-type voltage-gated calcium channels (Cav2.2) and transmitter release by collapsin response mediator protein-2 (CRMP-2) in sensory neurons. J Cell Sci 2009;122:4351–62.
[61] Wang Y, Brittain JM, Wilson SM, et al. Emerging roles of collapsin response mediator proteins (CRMPs) as regulators of voltage-gated calcium channels and synaptic transmission. Commun Integr Biol 2010;3:172–5.
[62] Schechter I, Butler PD, Jalbrzikowski M, et al. A New dimension of sensory dysfunction: stereopsis deficits in schizophrenia. Biol Psychiatry 2006;60:1282–4.
[63] Kantrowitz JT, Butler PD, Schecter I, et al. Seeing the world dimly: the impact of early visual deficits on visual experience in schizophrenia. Schizophr Bull 2009;35:1085–94.
[64] Hui Li, Sen Xia H, Shu Tang An, et al. Stereopsis deficits in patients with schizophrenia in a Han Chinese population. Sci Rep 2017;7:45988.
[65] Chang EF, Merzenich MM. Environmental noise retards auditory cortical development. Science 2003;300:498–502.
[66] Stern EA, Maravall M, Svoboda K. Rapid development and plasticity of layer 2/3 maps in rat barrel cortex *in vivo*. Neuron 2001;31:305–15.
[67] Crepel F. Regression of functional synapses in the immature mammalian cerebellum. Trends Neurosci 1982;5:266–9.
[68] Kuhl PK. Brain mechanisms in early language acquisition. Neuron 2010;67:713–27.

Yuan Zhang received her Ph.D. degree in Cognitive Neuroscience/Psychology from the State Key Laboratory of Cognitive Neuroscience and Learning, Beijing Normal University in 2020. Her research interest focuses on neural circuitry mechanisms underlying sensory processing functions and early experience-induced critical period plasticity of the mouse primary visual cortex.

Xiaohui Zhang is a professor of the State Key Laboratory of Cognitive Neuroscience and Learning, Beijing Normal University and a principal investigator (PI) of IDG/McGovern Institute for Brain Research. During 2003–2013, he was a PI at the Institute of Neuroscience, Chinese Academy of Sciences. The research of his laboratory is mainly focused on elucidating neural circuitry mechanisms underlying cortical sensory processing and early experience-dependent critical period plasticity, as well as hippocampus-dependent learning function.